Scattering of a Crystalline Gel Network: A New Organogel Based upon a Benzohydroxamic Acid Derivative

P. Terech,*,†,‡ A. Coutin,‡ and A. M. Giroud-Godquin†,§

Laboratoire Physico-Chimie Moléculaire, UMR 585, and SCIB-CC, CNRS URA1194, Département de Recherche Fondamentale sur la Matière Condensée, C.E.A-Grenoble, 17, rue des Martyrs, 38054 Grenoble Cédex 09, France

Received: January 30, 1997; In Final Form: June 23, 1997[⊗]

A new aromatic gelator, *p*-octylbenzohydroxamic acid (OBHA), forms thermoreversible networks for concentrations as low as ca. 0.1% in several organic liquids. In the context of organogelators, the OBHA originality consists of a chemical structure that combines aromaticity with hydroxyl and amine groups. Preliminary rheology studies qualify the system as a viscoelastic solid and characterize the gel to sol melting transition. The small-angle scattering techniques (X-rays and neutrons) are used to investigate the structural features of the aggregates and their junction zones in the network. OBHA molecules are associated through hydrogen bonds in reverse configuration within long and rigid fibers with circular ($r \approx 58$ Å) or slightly rectangular (ca. 70×150 Å) cross sections. A large-angle Bragg peak (spacing of 34.3 Å) characterizes the crystallinity of the network organized through bimolecular associations. The low-angle scattering of such crystalline gels can be described using the Debye−Bueche model assuming a random distribution of the heterogeneities in the network. Scattering data suggest the existence of a concentration-dependent growth process of lamellar-like junction zones.

1. Introduction

Among the low-molecular weight compounds known to exhibit a thickening or a gelling activity of organic liquids,[1,2] a large part of them have molecular structures appropriate for the emergence of intermolecular H-bonds. Nevertheless, despite that this mechanism of aggregation is largely represented, it is not unique, and other modes can be encountered involving, for instance, coordination bonds, overlap of unsaturated polarized sites, etc. Specific concentration-temperature and solvent conditions are required so that the autoassociation of the small gelator molecules proceeds into entangled colloidal structures. Thermoreversible three-dimensional (3D) networks are formed through a spectacular sol to gel phase transition which can involve a low quantity of gelator as low as ca. 0.1 wt %.

Such organogels exhibit common physical trends together with peculiar properties due to the chemical specificity of the gelator−organic liquid system. The gel-forming systems can be sorted according to (i) the chemical structure of the gelators, (ii) the type of structures and molecular orderings found within the networks, (iii) the type of liquids that can be gelled, (iv) the type of mechanical properties exhibited by the equilibrated materials, etc. Up to now, about 12 generic chemical types of molecules are known to have a gelling ability of organic liquids.[1,2] The field of organogelators is in constant development as demonstrated by the increasing number of discoveries. The expansion of the discovery rate of new organogelators is due to the combination of the improvement of appropriate techniques for their investigation (especially scattering techniques using intense radiation sources, see below) and a clarification of the physical concepts that can be used to describe these heterogeneous materials. In parallel, the applied field is more developed (lubrication, transportation of drugs, host−guest signal-responsive chemistry, sensors, etc., which use some specific properties of the gels such as molecular recognition, hindered diffusion in porous gel media, thermoreversibility of the mechanical properties, and other thermal, acoustic, optical, or electronic conduction properties.

Three chemical classes of organogelators proceeding through H-bonds can be isolated: fatty acids, substituted aromatic compounds, and steroid derivatives. As a representative of the first category, 12-hydroxy octadecanoic acid (see Chart 1, compound **II**) is a gelator of many polar and apolar saturated or unsaturated organic liquids.[3,4] For the second type, different aromatic gelators with hydroxyl groups are known such as amino acids,[5,6] benzylidenesorbitol derivatives[7] (see Chart 1, compound **III**), etc. and can gel various alkanic and alcoholic organic liquids. The third type of organogelators considered for reference is an androstanol derivative possessing both the hydroxyl and amine functions (see Chart 1, compound **IV**) as potential sites for H-bonds[8,9] that gels apolar saturated hydrocarbons. The gelling ability of the steroid is extremely sensitive to the presence of unsaturated bonds either in the organic liquid or within specific parts of the gelator molecule itself. These three examples of hydroxylated organogelators emphasize the great variety of structures that can be efficient to form gels with organic liquids. Nevertheless, trivial constitutive chemical features compulsory for organogelation are identified such as the presence of long aliphatic tails, the presence of at least two potential sites for molecular connection, and a certain resistance to crystallization. More refined molecular requirements can be recognized within a given class of organogelators. For instance, with functionalized steroids,[1,10−12] various key structural features can be examined such as the influence of (i) the α/β stereochemistry at C-3 of the steroid, (ii) the nature of alkyl chains on C-17 of the steroid ring, and (iii) their length and functionality upon the gelation ability. In numerous situations, gelators exhibit some outstanding intrinsic properties in their neat condensed phases, which can be retrieved in some of the structural features and properties of the related gels. As

* Author to whom correspondence should be addressed.
† Members of CNRS.
‡ Laboratoire Physico-Chimie Moléculaire.
§ SCIB-CC.
⊗ Abstract published in *Advance ACS Abstracts,* August 15, 1997.

S1089-5647(97)00371-4 CCC: $14.00 © 1997 American Chemical Society

CHART 1

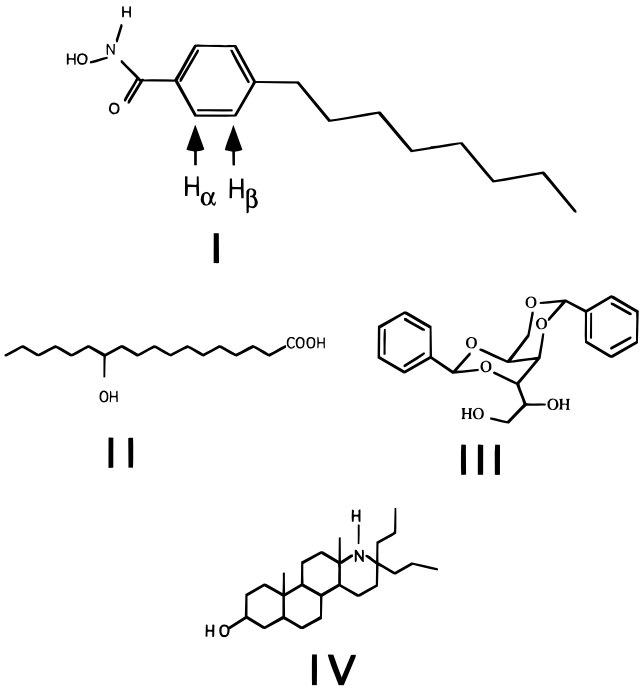

[a] **I**: *p*-octylbenzohydroxamic acid (OBHA). Positions α and *β* of the aromatic protons are indicated. "Reference" hydroxylated systems: **II** = 12-hydroxyoctadecanoic acid; **III** = benzylidenesorbitol; **IV** = androstanol derivative (see text).

example, some compounds, known to exhibit a discotic thermotropic mesophase, can also swell in appropriate solvents to separate the columnar arrangements and give entangled molecular threads in the semidilute range.[2] So far, thermotropism or optical activity are not, in organic solvents, parameters that are prerequisites to the gelation phenomenon. As example, organogelators are also known[2] that are racemic or non optically active or that do not exhibit any thermotropism.

Structural features such as aromaticity and the presence of hydroxyl, amine groups, and long aliphatic tails characterize any of the above hydroxylated reference systems. Consequently, it appears interesting to investigate the properties of a novel organogelator molecule (*p*-octylbenzohydroxamic acid, see Chart 1, compound **I**), which has the unique particularity of combining the three structural parameters. Implications of such a situation on the structures of the colloidal aggregates of the organogels are presented.

Hydroxamic acids are known to act as bidentate ligands and are frequently used as chelating agents for most coordination metals and actinides.[13] A new hydroxamic acid (*p*-octylbenzohydroxamic acid, abbreviated as OBHA), substituted by long alkanic chains, has been synthesized and gels most apolar hydrocarbons. Originally prepared in the perspective of liquid crystalline properties with a specialized chelation ability for bulky metals, the discovery of the gelling property of OBHA was serendipitous and emphasizes the somewhat enigmatic relationships between the chemical structure of a gelator and the long-range organizations found in the gel network. Due to the extreme fragility of the hydrocarbon-based networks (constituted by more than 99% solvent) made up of low-molecular weight compounds, the present study discards investigation techniques with aggressive preparation steps. The different stages of restructurations undergone by fibrillar aggregates when submitted to brutal observation procedures have been studied with the chiral androstanol **IV** (see Chart 1) gel and constitute a demonstrative example.[14] These modifications were induced by the mechanical stress generated by the solvent meniscus migration within the shrinking gel during the course of a shadowing replication electron microscopy method. To observe the genuine swollen gel in almost unperturbed conditions, small-angle scattering techniques (SAS) have been preferred since they allow a nondestructive and direct examination of the heterogeneous and dispersed systems. SAS techniques have proved to be essential for the structural study of many colloidal systems.[15,16] In the present work, structural characterizations (SAS) of the OBHA-hydrocarbon gels are completed with preliminary rheological, infrared (IR), and nuclear magnetic resonance (NMR) spectroscopic observations. A mechanism of formation of the 3D gel network and evolution with OBHA concentration is proposed.

2. Experimental Section

A suspension of 1 g (0.0015 mol) of hydroxylamine hydrochloride, 1.6 g (0.02 mol) of $NaHCO_3$ in 10 mL of ether and 10 mL of water was cooled to 1 °C. Two grams (0.1 mol) of *p*-octylbenzoic acid chloride (obtained by reaction of thionyl chloride with *p*-octylbenzoic acid) diluted in ether was added dropwise. After stirring overnight, the reaction mixture was filtered (yield was 60%, mp = 115 °C). Analysis calculated for $C_{15}H_{23}NO_2$: C, 72.25; H, 9.30; N, 5.62. Experimental: C, 71.97; H, 8.99; N, 5.32.

The nongelling *N*-methyl derivative of OBHA used the same procedure as above with *N*-methylhydroxylamine hydrochloride instead of hydroxylamine hydrochloride (mp = 66 °C). Analysis calculated for $C_{16}H_{25}NO_2$: C, 72.95; H, 9.57; N, 5.32. Experimental: C, 73.02; H, 9.62; N, 5.27.

Mixtures of solid OBHA and organic liquids (cyclohexane, benzene, carbon tetrachloride, etc.) were heated until clear liquids were obtained. The homogeneous warmed solutions were cooled to room temperature to induce the gel formation. The self-supporting gels were white, opaque, and stable while the most dilute samples were slightly shrunk to expel small amounts of clear liquid. The gels were prepared directly within 1 mm thickness quartz cells for the small-angle neutron-scattering (SANS) experiments in deuterated liquids. For small-angle X-ray-scattering (SAXS) experiments, gels were introduced in 1 mm cells with capton windows. Xerogels were solids obtained by slow evaporation of the solvent.

SAXS data were obtained at the D.C.I. synchrotron source, "Laboratoire pour l'Utilisation du Rayonnement Electromagnétique" (LURE, Orsay, France), on the D22 instrument at a wavelength $\lambda = 1.458$ Å ($E = 8500$ eV) and two distances (1.75 and 0.714 m). A gas-filled ($Xe-CO_2$) detector with a 0.217 mm per channel spatial resolution was used (512 channels). Data were transmission corrected for the empty beam signal and solvent scattering according to $I = I_{sam}/(I_{0\,sam}T_{sam}t_{sam}) - I_{back}/(I_{0\,back}T_{back}t_{back})$, where the subscripts sam and back refer to the sample and background respectively, t is the corresponding counting time, I_0 is the incident X-ray intensity, and T is the transmission. The momentum transfer Q (Å^{-1}) was defined as $Q = (4\pi/\lambda)\sin\theta$, as usual for elastic scattering, where θ is half the scattering angle and λ the wavelength of the incident radiation. The Q-range investigated was 0.005−0.3 Å^{-1}.

SANS experiments used the PAXE spectrometer (Laboratoire Léon Brillouin, Orphée reactor, Saclay, France) within the 0.006 Å^{-1} < Q < 0.35 Å^{-1} Q-range. A two-dimensional BF_3 multidetector of dimension 64 × 64 cm^2 with 1 × 1 cm^2 cells in a planar square matrix arrangement was used ($\Delta\lambda/\lambda \approx 0.10$). Usual corrections for background subtraction, transmission, and normalization were applied.[18]

The rheology experiments, made in the linear regime of deformations, used a stress rheometer Haake RS100 in the

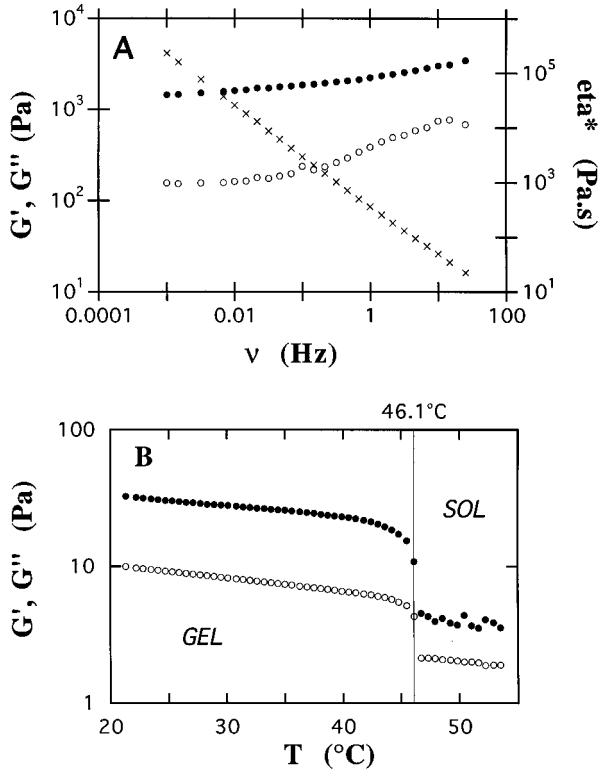

Figure 1. Rheology of OBHA gels in dodecane. (A) Frequency dependence of rheological parameters ($G'(\nu)$, ●; $G''(\nu)$, ○, $\eta^*(\nu)$, ×) for a gel ($C = 1.36$ wt %) submitted to a constant applied stress $\sigma =$ 10 Pa in a linear rheological regime. The parameters are calculated[28] from the phase lag between the applied shear stress and the related flow and from the ratio of the amplitudes of the imposed oscillation to the response of the gel. G', G'', and η^* are linked together following $|\eta^*(\omega)| = [G'^2(\omega) + G''^2(\omega)]^{1/2}/\omega$, where ω is the angular frequency ($\omega = 2\pi\nu$). (B) Investigation of the melting transition of a gel ($C =$ 0.45 wt %). An oscillatory ($\nu = 1$ Hz) constant shearing stress ($\sigma = 5$ Pa) is applied while the sample is progressively heated to the sol phase. The sharp variation of G' (●) and G'' (○) defines the domains of existence of the sol and gel phases.

frequency range 0.001−61 Hz. A plate−plate geometry was used (20 mm diameter, 0.25 mm gap) with serrated surfaces so as to prevent sliding due to the liquid film expelled by some dilute samples. A special device was used to limit any solvent evaporation (dodecane: $E = 216$ °C). Temperature was regulated with an accuracy better than 0.1 °C.

The NMR characterization used a Bruker AC200 spectrometer equipped with a 5 mm dual probe operating at 200.13 MHz for the proton. 1D spectra were recorded at temperatures ranging from 293 to 350 K. The infrared (IR) spectra were obtained with a single-beam FTIR Perkin Elmer 1600 spectrometer. Spectra were obtained with four scans at 4 cm^{-1} resolution in the 4000−400 cm^{-1} wavenumber range. The OBHA powders (crystals and xerogels) were studied as potassium bromide pellets while solutions and gels were investigated in a cell with fluorine windows.

3. Results

A preliminary rheological characterization of OBHA/dodecane samples is shown in Figure 1. Figure 1A displays the frequency dependence of the elastic modulus *(G′)*, loss modulus *(G″)*, and complex viscosity *(η*)* for an equilibrated OBHA sample (concentration $C = 1.36$ wt %). Figure 1B shows the temperature dependence of the G', G'' mechanical parameters of a sample progressively heated to a liquid state during a temperature-sweep experiment.

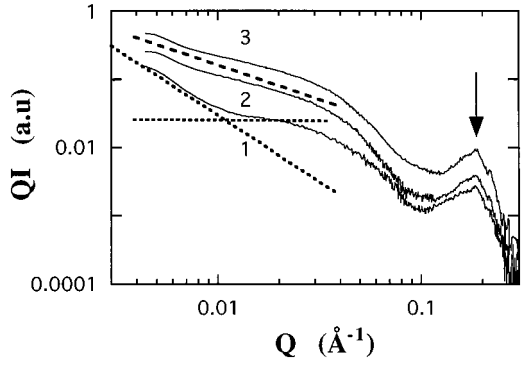

Figure 2. SAXS of OBHA gels in dodecane. *QI vs Q* logarithmic plots (see text) for three samples (1, $C = 0.32$ wt %; 2, $C = 1.14$ wt %; 3, $C = 2.12$ wt %). In the low-angle region, the dotted lines are reference slopes (−2.2 and 0) for the cross-sectional intensity decay around the low-angle turn-up of curve 1. The dotted line between curves 2 and 3 is a reference slope −1. In the large-angle region, the arrow points at a broad Bragg peak ($Q \approx 0.183$ Å^{-1}).

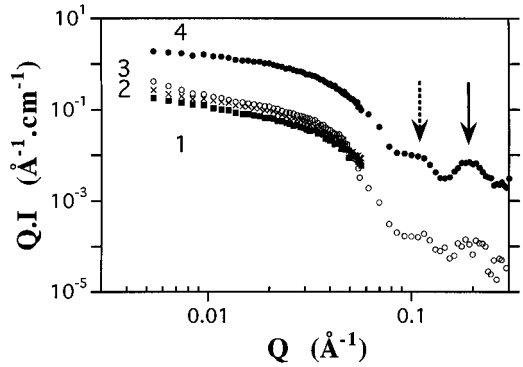

Figure 3. *QI vs Q* SANS logarithmic plots of OBHA gels in deuterated cyclohexane (1, ■, $C = 0.11$ wt %; 3, ○, $C = 0.66$ wt %; 4, ●, $C =$ 2.9 wt %) and benzene (2, ×, $C = 1.0$ wt %). At large angles, the dotted arrow ($Q \approx 0.102$ Å^{-1}) points at a marked bump in the intensity decay while the bold arrow indicates a broad Bragg peak (at $Q \approx 0.184$ Å^{-1}).

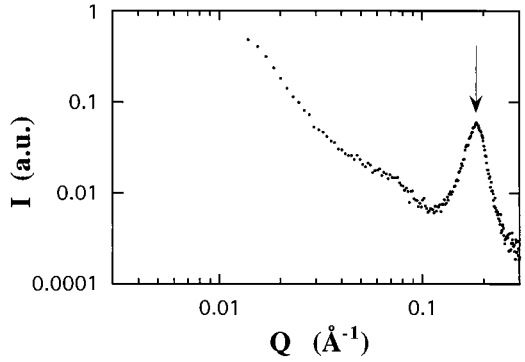

Figure 4. *I vs Q* SAXS profile of the OBHA solid used for the preparation of the organogels. The arrow indicates an intense Bragg peak at $Q \approx 0.183$ Å^{-1}.

Figure 2 shows the concentration dependence of the SAXS curves of OBHA organogels. A specific representation, *Q·I vs Q*, is used and detailed below. SANS is used as a complementary technique, and Figure 3 collects the scattering curves of four representative OBHA gels. For comparisons with the scattering of OBHA gels, Figure 4 presents the SAXS curve (in the same *Q*-range) of the powder used to prepare the samples.

Figure 5 compares the NMR spectrum of a OBHA liquid solution (deuterated chloroform, spectrum A) in nongelling conditions to that of a warmed deuterated cyclohexane solution

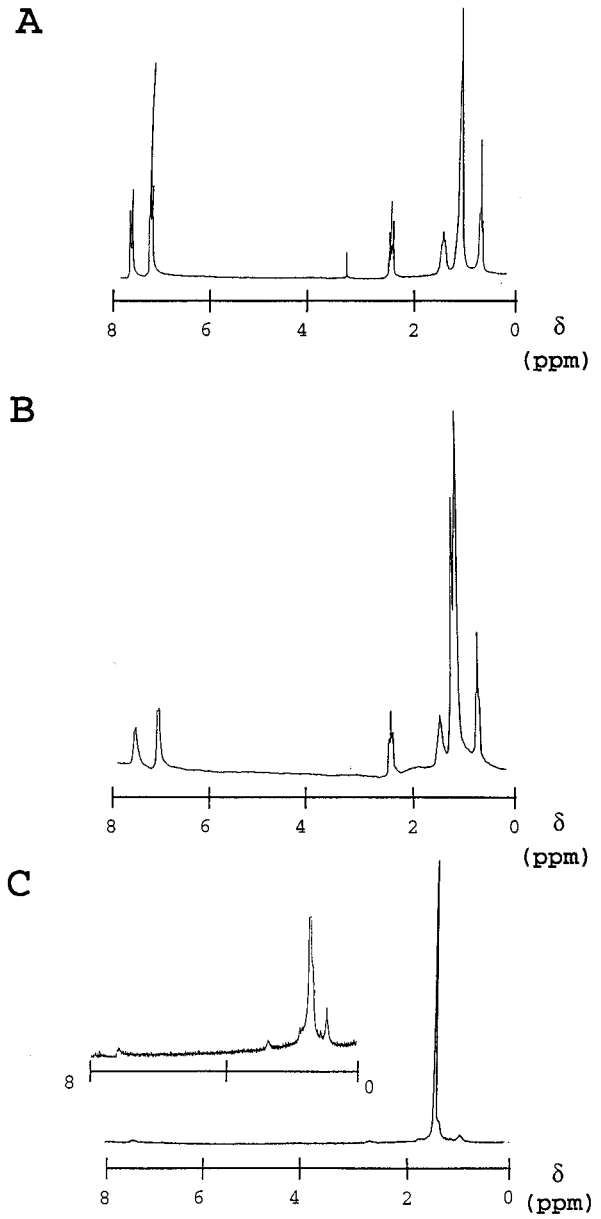

Figure 5. NMR spectra of OBHA solutions and gels. (A) Solution in deuterated chloroform at room temperature ($C \approx 0.5$ wt %). (B) OBHA liquid solution at $C = 1.5$ wt % in deuterated cyclohexane at $T = 77$ °C. (C) Gel at $C = 1.5$ wt % in deuterated cyclohexane at $T = 20$ °C (inset is the enlarged spectrum). The peak at 1.4 ppm in spectra B and C is due to a C_6-H_{12} remainder in C_6D_{12}.

(spectrum B) and to that of the corresponding gel phase (spectrum C) obtained by cooling the preceding sample to room temperature.

H-bonded hydroxyl groups are known to exhibit broad bands, corresponding to the OH stretching vibration, in the wavenumber range 2800−4000 cm^{-1} (while other regions of the spectrum can also be instructive). Due to the lack of significant IR absorption within the above wavenumber range, carbon tetrachloride was used as a convenient solvent to demonstrate the implication of H-bonding mechanisms in the gelation phenomenon.[19] Figure 6 shows the 2000−3500 cm^{-1} part of the most significant spectra: OBHA gels in CCl_4 (A) at two temperatures (A1, A2); reference spectra (B) useful for the identification of the bands (B1 = C_8H_{17}−Ph−CON(OH)(CH_3), B2 = C_9H_{19}−Ph−CONH(OK), B3 = Ph−CONH(OH), solids in KBr pellets); OBHA solids (C) i.e. crystalline powder (C1) and xerogel (C2).

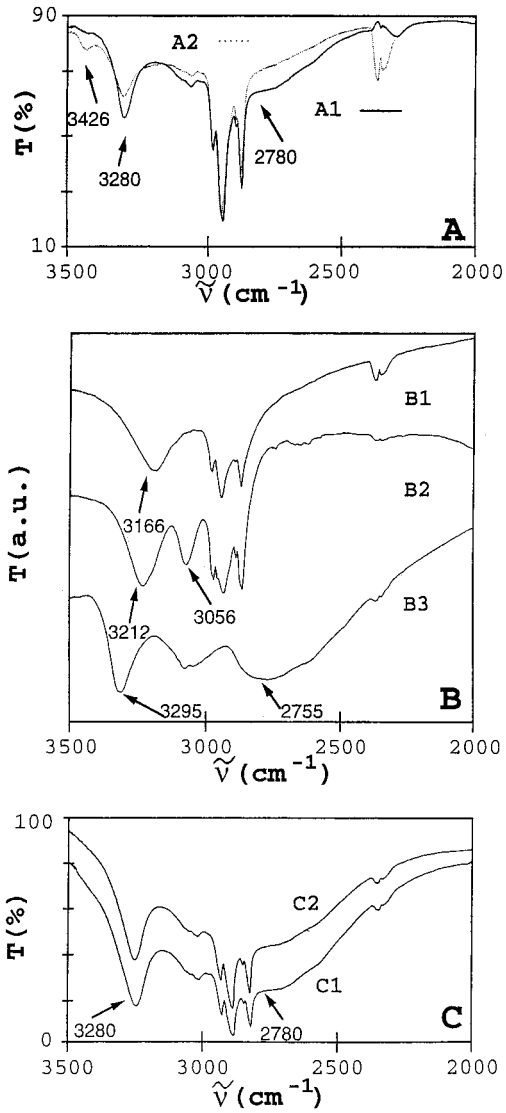

Figure 6. FTIR spectra of OBHA gels and solids (crystalline solid and xerogel) and analogous derivatives. (A) OBHA gels in CCl_4 at two temperatures, $C = 0.7$ wt % (A1, $T = 20$ °C; A2, T ca. 50 °C). (B) Reference spectra of analogous solids (B1 = C_8H_{17}−Ph−CON(OH)(CH_3), B2 = C_9H_{19}−Ph−CONH(OK), B3 = Ph−CONH(OH). (C) OBHA solids (C1, crystalline powder; C2, xerogel).

4. Analysis and Discussion

The equilibrated material obtained through cooling of a warmed homogeneous OBHA hydrocarbon solution behaves as a solid-like system (Figure 1A). The storage modulus $G'(\nu)$ (G'(1 Hz) = 2300 Pa at $C = 1.36$ wt %) extends as a plateau over almost 5 decades of frequencies (ν) and is significantly larger than the corresponding loss shear modulus $G''(\nu)$ (G''(1 Hz) = 380 Pa). Although the $G''(\nu)$ profile is slightly sloped, the longest relaxation time is of the order of 10^3 s so that the system behaves as a solid on long time scales (at least hours). These mechanical characteristics confirm the visual observations of the elastic and resilient characters of the OBHA/hydrocarbon system, which can be described as a self-supporting gel.[20] The hydrocarbon-based OBHA gels are thermoreversible systems that can be cycled between the sol and gel states by heating and cooling ramp sequences. A large hysteresis of the phase transition is observed (not shown). A gel can be progressively equilibrated at a temperature in the gel domain of the phase diagram and up to a point, the melting temperature, at which only the sol phase is stable as shown in Figure 1B. The gel network is progressively denatured by the heating procedure,

and the elasticity decreases regularly toward a sharp drop down at the melting transition. The "melting temperature" (46.1 °C at $C \approx 0.45$ wt %) separates the rheogram in two domains defining the existence of the gel and solution states (or sol state defined as a dispersion of nonconnected small aggregates). A gel put at a temperature higher than its "melting temperature" is unstable and liquefies to the sol phase through a sharp transition. For temperatures in the gel domain, i.e. less than the "melting temperature", the OBHA solution is a supersaturated solution that is unstable and that stabilizes through aggregation reactions. At this stage, the OBHA dispersion at high temperature in dodecane, subsequently cooled, is a viscoelastic solid of the thermoreversible gel type.

Values of the elastic modulus can be compared to other organogels behaving as viscoelastic solids. For instance, the mentioned "reference" fatty acid system (see Scheme, compound **II**) in identical experimental conditions exhibits also a large elasticity value $G'(1\text{ Hz}) = 8220$ Pa (while $G''(1\text{ Hz}) = 560$ Pa at $C = 1.27$ wt %). It has been shown that this fatty acid network is made of long and rigid fibers interconnected into crystalline microdomains[4] with a monoclinic symmetry. The cross-sectional shape of the fatty acid fibers, as well as the morphology of their "junction nodes" in the gel network, was found to be dependent upon the type of organic liquid (between benzene, hexafluorobenzene or cyclohexane). Concerning the OBHA gels, the measured elasticity is also relatively large and questions the structural nature of the OBHA aggregates and the type of their connections in the gel network.

The SAXS profiles of the OBHA gels (Figure 2) show 3 decades of the intensity decrease over 2 Q-decades. From the minimal Q-value (0.004 Å^{-1}) to $Q \approx 0.03$ Å^{-1}, a monotonous decrease ($d(QI)/dQ \approx -0.9$) is observed for gels at $C > 1$ wt %. The scattering curve for the most dilute sample ($C = 0.32$ wt %) is different in this low-angle domain and clearly exhibits a change of the slope $d(QI)/dQ$ at $Q \approx 0.01$ Å^{-1}. Just around this inflection point, the profile varies from $d(QI)/dQ \approx -2.2$ to $d(QI)/dQ \approx 0$. At larger Q-values (ca. 0.03 Å$^{-1} \leq Q \leq 0.1$ Å^{-1}), and for all reported concentrations, the intensity sharply decays and precedes a broad and intense peak (or combination of peaks) around $Q \approx 0.184$ Å^{-1}.

The observation of a low-angle scattering signal is trivial evidence[15,16] for the existence of colloidal aggregates in OBHA organogels. Since the initial warmed solution consists of dispersed low-molecular weight OBHA molecules, the signal arises from macromolecular species resulting from aggregation reactions taking place once the system is put under the conditions of the equilibrium gel phase. The procedure to prepare the gels is such that, for a given concentration (beyond a minimum value $C_{\min}^{\text{gel}}$), a transition from the solution to the gel state is initiated by lowering the temperature. The rheological study of the gel to sol phase transition (Figure 1B) characterizes the thermal behavior of the colloidal system. The 3D arrangement of the aggregates is thermoreversible and equilibrates by thermal equilibrium reactions. The concentration dependence of the asymptotic SAXS behaviors of OBHA gels further indicates that the aggregation reactions may follow complex schemes from, first, isolated molecular species (no low-angle scattering signal) to connected large aggregates (Figure 2, curve 1) and, second, from aggregates to further aggregated colloidal structures (Figure 2, curves 2, 3).

For the most dilute gel (Figure 2, curve 1), the combined observation of a QI plateau within a restricted Q-domain together with a subsequent sharp intensity decrease at larger angles suggests interpreting this part of the curve in terms of a form factor for fibrillar structures. It is known[21,22,23] that the low-angle scattered intensity for isolated rodlike aggregates, is given by expression 1, (Expression 1 is an expansion in the low-angle limit of $I(Q) = (\pi L/Q)[A\Delta\rho\ (2J_1(Qr))/Qr]^2$, where J_1 is the Bessel function of the first kind and A the cross-sectional area of the rodlike scatterer of length L.)

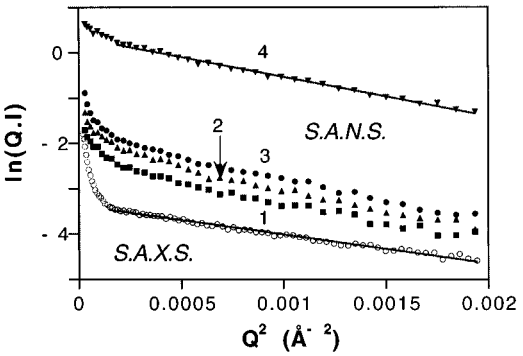

Figure 7. Gaussian cross-sectional intensity decays $\ln(QI)$ *vs* Q^2, which reveal the fibrillar structure of the OBHA aggregates. From the straight lines, the radii (r) for cylindrical fibers are deduced (see expression 1). SANS: $r = 58$ Å, (1) $C = 0.11$ wt %, cyclohexane; (2) $C = 1.0$ wt %, benzene; (3) $C = 0.66$ wt %, cyclohexane; (4) $C = 2.9$ wt %, cyclohexane. A weak extrascattering is seen in the innermost part of the curves and discussed in the text. SAXS: (○) dodecane, $C = 0.32$ wt %, $r = 50$ Å.

$$I = \frac{\phi(\pi r \Delta\rho)^2}{Q} \exp(-Q^2 r^2/4) \qquad (1)$$

ϕ is the gelator concentration (or volume fraction of rods), $\Delta\rho$ is the volume contrast of the aggregate relative to the surrounding medium (i.e. the difference of electron (or neutron scattering length) density between the rod and the embedding liquid medium), and r is the radius of the rodlike scatterer (corresponding to the cross-sectional radius of gyration $r_c = r/\sqrt{2}$).

In the very low-angle limit, expression 1 expands as a Q^{-1} intensity decay (a plateau in a QI *vs* Q representation), followed, at larger angles, by a sharp Gaussian decay due to the finite size of the cross section of the fibers. As mentioned above, these scattering features are experimentally observed for the dilute OBHA gel and support the model of a colloidal network of fibers.

Following expression 1, the radius of the fibers can be estimated using $\ln(QI)$ *vs* Q^2 plots with SAXS and SANS data. Figure 7 shows that linear variations are observed in the range 0.012 Å$^{-1} < Q < 0.05$ Å^{-1}. From the corresponding slopes within appropriate Q-ranges (ca. $Qr_c \leq 1$), values for the cross-sectional radii of equivalent homogeneous cylindrical rods can be estimated.[21,23] Despite a certain dispersion, the values $r_{\text{SAXS}} \approx 50 \pm 3$ Å and $r_{\text{SANS}} \approx 58 \pm 3$ Å are estimated, and their difference is discussed below as a contrast effect of the OBHA aggregate with respect to the radiation used.

The OBHA gels exhibit a solidlike rheological behavior with significant elasticity (Figure 1A) and yield stress values (not shown). Such a behavior suggests that the connection zones of the network are long lifetime microdomains. In addition, the wide-angle region of the curve shows a broad and intense peak, comparable to that observed with the OBHA powder (Figure 4) and which is symptomatic of the existence of ordered microdomains. These indications suggest that crystalline microheterogeneities constitute the connection sites of fibers in the network (junction zones or nodes). As already shown in Figure 2 (curve 1), the typical QI plateau for linear aggregates is restricted in the low-angle region by a $Q^{-3.2}$ scattering component (in a I *vs* Q representation). This latter can be interpreted as the low-angle scattering "signature" of the

microheterogeneities responsible for the broad Bragg peak at larger angles ($Q \approx 0.183$ Å^{-1}).

The inhomogeneous distribution of the microcrystalline junction zones can be modeled using the Debye−Bueche random-two-phase model.[24] The heterogeneities are distributed according to an exponential correlation function (expression 2).

$$\gamma_0(r) = \exp(-r/d) \qquad (2)$$

In expression 2, d is the correlation length and reflects the average size of the heterogeneities of volume fraction ϕ and r is the radial distance in the system. The corresponding scattering contribution in the Q-reciprocal space (I_{DB}) is obtained by an appropriate Fourier transformation[23] and reads

$$I_{DB}(Q) = 8\pi\phi_{nodes}(1 - \phi_{nodes})(\Delta\rho)^2 \frac{d^3}{(1 + d^2Q^2)^2} \qquad (3)$$

The OBHA gel network is described as a 3D mesh of fibers connected in crystalline solid-like microdomains with a random size distribution. The pronounced experimental slope (dI/dQ ≈ -3.2) of the low-angle extrascattering observed for the OBHA gel at $C = 0.32$ wt % compares to the expected theoretical Q^{-4} scattering of the Debye−Bueche component.

To summarize, the scattering curve of a OBHA organogel consists of three components observable in three distinct Q-regions: (i) a low-angle term characterizing the distribution of the junction zones, (ii) form factor term(s) describing the connected aggregates, and (iii) large-angle Bragg peak(s) due to molecular orderings within the aggregates (nodes and fibers). Such a scattering pattern is frequently found in this class of low-mass organogelators.[2] Concerning OBHA organogels, the three components are clearly seen in Figure 2 (curve 1) with the typical sequence, from low to large angles: a low-angle Debye−Bueche bump, a Q^{-1} plateau followed by a sharp Gaussian decay, a broad peak at $Q \approx 0.18$ Å^{-1}.

Expression 3 shows that the amplitude of the Debye−Bueche component, originating from the distribution of the nodes, depends on their volume fraction (ϕ_{nodes}) and more strongly on their size d. The related influence upon the low-angle part of the scattering curve can be dramatic as shown in the Appendix (Figure 11). In the crossover Q-region between the low-angle extrascattering and the Q^{-1} plateau, a subtle distinction between the influence of d and ϕ_{nodes} upon the scattering curve is noticed but not used in the present analysis. The contrast ($\Delta\rho$) of the nodes with a volume fraction ϕ_{nodes} is taken to be similar to that of the connected fibers since the nodes result from the juxtaposition or fusion of OBHA fibers. Nodes and fibers contrast similarly with the embedding solution in which the concentration of isolated OBHA molecules is certainly low. It is known that the critical micelle concentrations[25] (cmc) or the average aggregation numbers[26] of finite micelles of autoassociative molecules in nonpolar organic solvents are very low. The growth of infinitely long rodlike aggregates is very sensitive to the concentration and temperature since the related molecular weight distribution results from thermal equilibrium of aggregation reactions in accordance with mass-action principles. The suspensions of long OBHA fibers do not evolve toward phase separation, as thermodynamically expected,[27] thanks to the rigid connections (or nodes) developed in the 3D network.

Good agreement of expression 3 with the SAXS data is obtained in Figure 8 (curve 1). At this stage, values of parameters ϕ_{nodes} and d are estimated from the innermost part of the scattering curve. In future work, an evaluation of the network crystallinity could take advantage of correlations between both the low-angle (Debye−Bueche analysis) and large-angle (amplitude width of the Bragg peak) parts of the scattering curves.

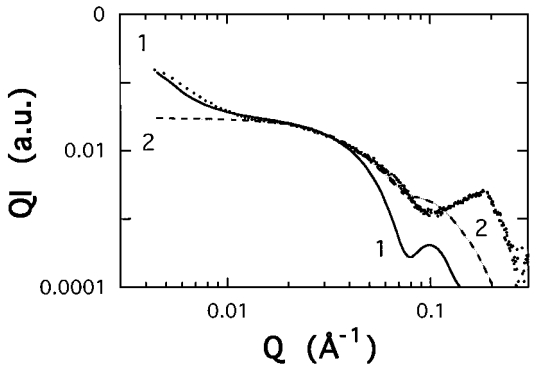

Figure 8. SAXS of a OBHA gel in dodecane at $C = 0.32$ wt % (●). Full line (1) is the theoretical scattering of a fibrillar system (expression 1) with heterogeneities described by a Debye-Büeche component (expression 3) with $d = 500$ Å, $\phi_{nodes} = 0.001$, $r = 50$ Å, and a radial polydispersity $\epsilon = 0.15$. The comparison must be made up to the start of the Gaussian decay since at larger angles, the broad peak is not taken into account in the model. Dotted line (2) shows the theoretical scattering (two-component model) in the large-angle region modified by a population of thinner fibrils ($r = 17.5$ Å, fraction = 0.5) without heterogeneities.

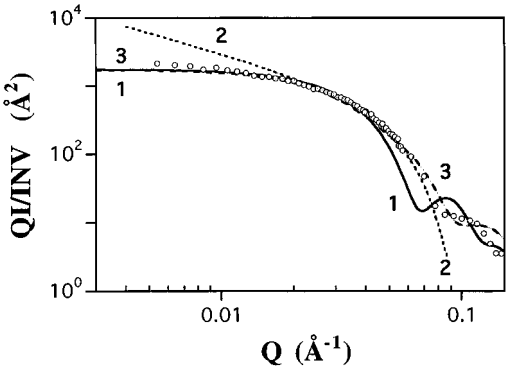

Figure 9. SANS of a OBHA gel in deuterated cyclohexane ($C = 1.5$ wt %). Cross-sectional intensity normalized by the scattering invariant INV. Full line (1) is the theoretical scattering following expression 5 for fibers with a cylindrical symmetry ($r = 58$ Å, $\epsilon = 0.15$). Dotted line (2) is the theoretical scattering for lamellar aggregates ($T = 70$ Å, $\epsilon = 0.1$). Dashed line (3) is the theoretical scattering for fibers with rectangular cross section (ca. 70 × 150 Å, $\epsilon = 0.15$).

Neutron-scattering curves (Figures 3, 9) are used to validate and complete the analysis in the three Q-domains. For instance, for a gel at $C = 1.5$ wt % (Figure 9), the low-angle region appears as a monotonic decrease (dI/d$Q \approx -1.4$) slightly more sloped (dI/dQ ca. -1.9) in the innermost part ($Q < 0.008$ Å^{-1}). The intermediate Q-range shows a sharp intensity decrease (0.03 Å^{-1} < Q < 0.08 Å^{-1}) followed by an oscillation ($Q \approx 0.102$ Å^{-1}) and a broad peak at $Q \approx 0.183$ Å^{-1}. The small differences in the innermost extrascatterings of SANS and SAXS data are not detailed but could be related to the sensitivity of anchoring and germination mechanisms with the cell surfaces (quartz or capton). The concentration dependence of the SANS curves in the Q-range of the Gaussian decay (Figure 7) shows that the related cross-sectional sizes do not vary significantly. Consequently, the situation is favorable for the analysis of the formfactor component in the intermediate Q-range. A determination of the most probable shape of the individual aggregates is performed using a calibration method with the scattering invariant[23] (INV). According to expression 4, the integral of the intensity over the reciprocal space is related to the mean square fluctuation of the contrast. The integral (INV) is

independent of any other feature of the statistically isotropic colloidal system.

$$\mathrm{INV} = \int_0^\infty Q^2 I(Q)\, \mathrm{d}Q = (\Delta\rho)^2 \phi(1-\phi) 2\pi^2 \qquad (4)$$

ϕ is the volume fraction of the scatterers with a volume contrast $\Delta\rho$. Expression 5 combines expressions 1 and 4 and is used to determine the local geometry of the aggregates. The corresponding parameter (i.e. radius r for a rodlike geometry) is extracted without making any further assumption for the contrast of the aggregates.

$$\frac{Q \cdot I(Q)}{\mathrm{INV}} = \frac{r^2}{2(1-\phi)} \left(\frac{2J_1(Qr)}{Qr} \right)^2 \qquad (5)$$

Figure 9 shows the calculation made for two extreme geometries such as cylindrical fibers and lamellas. It shows that the position of the theoretical curve for cylindrical fibers with a radius $r =$ 58 Å (i.e. the intensity level and Q-location of curve 1) with respect to the data is correct. Curve 2 shows that the lamellar symmetry is not appropriate to describe the OBHA aggregates at this concentration ($C = 1.5$ wt %). The calibration by the invariant makes the agreement relying upon only one parameter, i.e. the radius of the rod, and is thus very powerful. It is concluded that the aggregates are fibers with a cross section close to the circular symmetry ($r = 58$ Å). Nevertheless, slight departures are noticed in the shape of the intensity decay (especially its curvature in the intermediate Q-range) and that can be illustrated, for instance, by comparing the exponents of the asymptotic low-angle power law for the decay ($I \approx Q^{-\alpha}$). It appears that the experimental value ($\alpha \approx 1.4$) is somewhat in between the theoretical value for rodlike scatterers ($\alpha \approx 1$, expression 1) and that for lamellas of thickness T ($\alpha \approx 2$) (The theoretical low-angle scattering[23] of a lamellar-like infinite aggregate (thickness T) is given by: $QI = (2\pi\ C\overline{\Delta b^2}\ M_A)/Q \exp(-Q^2 R_t^2)$, where R_t is the transverse radius of gyration ($R_t^2 = T^2/12$), $\overline{\Delta b}$ is the specific neutron contrast, C is the concentration (g/cm^3), and M_A is the molecular weight per unit area). This situation may reveal the existence of rectangular cross sections. Curve 3 shows the improvement obtained by using the theoretical form factor of ribbons with a rectangular (ca. 70 × 150 Å) cross section corresponding to a cross-sectional area identical to that for the circular shape (10 568 Å^2). Curves 1 and 3 are superimposed in the low-angle part, while the large-angle bump at ca. $Q \approx 0.102$ Å^{-1}, revealing relatively well-defined cross sections, is correctly reproduced by curve 3 as well as the intermediate Q-range curvature.

The analysis of the complete scattering curves and related Gaussian decays (Figure 7) reveals the inhomogeneity of the cross-sectional contrast profile. A Q-shift of the curves (SAXS, Figure 2, and SANS, Figure 3) is observed that corresponds to a variation of ca. 10 Å of the radii of the cylindrical symmetries. Slight absolute variations of r are observed to depend on the method used (invariant or $\ln(QI)$ *vs* Q^2 plots), in relation to the Q-range where the fit is performed, and/or the departure from the circular cross-sectional symmetry. It remains that the smaller diameter is measured with the X-ray radiation and may correspond to the oxygenated parts of segregated OBHA molecules within the fibers. The difference of ca. 10 Å is comparable to the length of the lipophilic part of OBHA, which suggests that fibers are coated with alkanic tails organized in reverse micellar organizations.

Additional information concerning the gelation phenomenon and the related molecular aggregation mechanisms can be gained both from ^{1}H NMR and FTIR preliminary studies. A "reference" spectrum is recorded under conditions in which no gelation can be observed in the dispersing liquid $CDCl_3$ (Figure 5A). Focusing for instance on the two doublets at 7.65 ppm (H_α) and 7.2 ppm (H_β), the observation of resolved resonances of the aromatic protons indicates that the OBHA molecules can freely rotate. Conversely, in controlled aggregative conditions, i.e. in warmed cyclohexane, these resonances are less resolved in the sol state where only small aggregates are present (Figure 5B). Eventually, in the gel phase at room temperature, the resonances of the aromatic protons and others are completely damped (Figure 5C) by a motional broadening. The effect is so severe that the signals are hardly detectable above the base line (see inset). During the aggregation phenomenon, the motion of the OBHA molecules involved within the fibers is dramatically reduced from the solution to the gel (through the sol state). Due to the nonaveraging of the magnetic anisotropies of the tensorial quantities describing the resonance of the protons (i.e. H_α, H_β), a solid-like spectrum is observed over a spread of resonance frequencies. Qualitatively, the freezing of motion of OBHA aggregates in the gel is consistent with the picture of fibers rigidly connected in crystalline-like microdomains.

IR spectroscopy (Figure 6A) reveals the spectral regions of importance in the aggregation/gelation phenomena. The quantity of OBHA aggregates results from thermal equilibrium reactions so that the lower the temperature *(T)*, the higher the content of OBHA aggregated species. Three regions can be noticed: a peak at 3426 cm^{-1} (rather weak, increasing with a T increase), a peak at 3280 cm^{-1} (decreasing with a T increase), and a very broad band at ca. 2780 cm^{-1} (decreasing with a T increase). Analogues are used to characterize the above vibrations typical of the OBHA organogelation. Figure 6B1 shows the spectrum of the *N*-methyl OBHA analogue (C_8H_{17}−Ph−CON(OH)(CH_3)): a striking consequence is the loss of the gelation ability. The spectrum shows a peak at 3166 cm^{-1} while that at 3280 cm^{-1} has disappeared. The potassium salt analogue C_9H_{19}−Ph−CONH(OK), which does not have a OH group, shows two peaks (Figure 6B2) at 3212 and 3056 cm^{-1} while the broad peak at 2780 cm^{-1} has disappeared. From these observations, it can be assumed that the band at 2780 cm^{-1} is a stretching OH bonded vibration. On the basis of these preliminary experiments, attributions can be proposed (stretching vibrations): broad band at ca. 2780 cm^{-1} = $\nu_{\mathrm{O-H\ bonded}}$, band at 3280 cm^{-1} = $\nu_{\mathrm{N-H\ bonded}}$, and band at 3426 cm^{-1} = $\nu_{\mathrm{N-H\ free}}$. Spectrum 6B3 confirms the spectral attributions since the analogue Ph−CONH(OH) presents two bands at 3295 and ca. 2755 cm^{-1}. It is interesting to note that Ph−CONH(OH) does not form gels in cyclohexane. The behavior is consistent with the assumed role of these chains as modulators of fiber−fiber interactions and inducers of bimolecular layered organizations within fibrillar aggregates. The OBHA structure is propitious for the development of intra- and intermolecular hydrogen bonds in gels and xerogels in a fashion very similar to the organization found in the solid state as shown in Figure 6C. Molecular simulations (not shown) indicate that various intra- and inter-associations can be drawn between the OBHA molecules with different orientations of the planar benzenic rings. Consistently, the SAXS data of the crystalline solid and the gel both exhibit an identical Bragg peak associated to the OBHA bimolecular length (see below), which is attributed to crystalline microdomains acting as the nodes of the solid-like network.

5. Conclusion

The rheological measurements have demonstrated that the material obtained through dissolution of OBHA at high temperatures in hydrocarbons is a gel with all properties of a

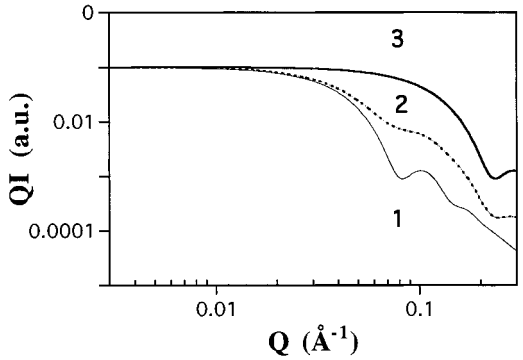

Figure 10. Theoretical SAS form factor curves for cylindrical long and rigid fibers. 1, one component, $r = 50$ Å, $\epsilon = 0.15$; 2, two-components, $r = 50$ Å, $\epsilon = 0.15$, volume fraction $\phi = 0.5$, and $r = 17.5$ Å, $\epsilon = 0.15$; 3, one component, $r = 17.5$ Å, $\epsilon = 0.15$.

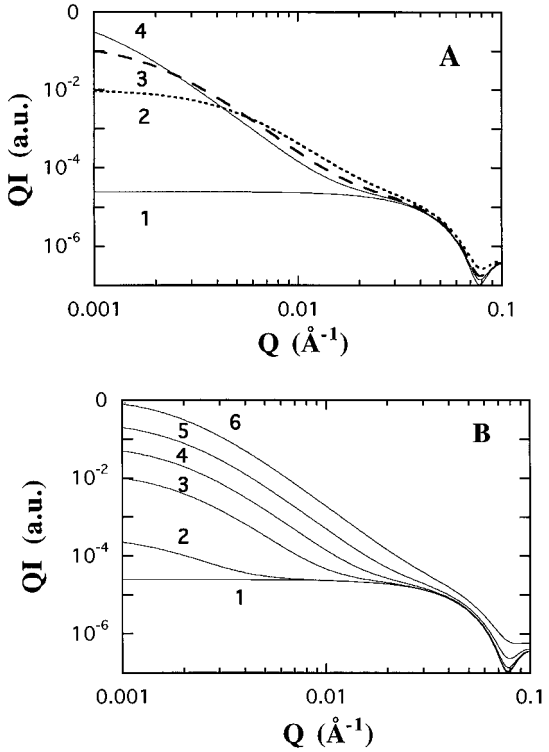

Figure 11. Small-angle scattering of a network with two types of scatterers: cylindrical fibers (component 1, $r = 50$ Å, $\epsilon = 0.1$) and randomly dispersed heterogeneities (component 2, correlation length d and volume fraction of nodes ϕ_{nodes}). (A) ϕ_{nodes} is kept constant to 0.05 while d is varied. Curve 1, $d = 0$ Å; curve 2, $d = 200$ Å; curve 3, $d = 500$ Å; curve 4, $d = 1000$ Å. (B) d is fixed to 500 Å while ϕ_{nodes} is varied. Curve 1, $\phi_{nodes} = 0\%$; curve 2, $\phi_{nodes} = 0.0001$; curve 3, $\phi_{nodes} = 0.005$; curve 4, $\phi_{nodes} = 0.025$; curve 5, $\phi_{nodes} = 0.1$; curve 6, $\phi_{nodes} = 0.4$.

viscoelastic solid. The binary system exhibits a sharp gel to sol melting transition at a temperature that is conveniently estimated by rheology. The gel can be formed at low OBHA concentrations ($C \approx 0.1$ wt %), and the SAXS and SANS techniques characterize the unidirectionality of the aggregates.

In a dilute system, the rigid fibers have a cross-sectional shape that is circular ($r \approx 58$ Å) or, more probably, slightly rectangular (ca. 70 × 150 Å). The mechanical response of the solid-like gel associated with the observation of a broad Bragg peak at $Q \approx 0.183$ Å^{-1} suggests that the network is rigidified by crystalline microdomains. The results can be examined with respect to the OBHA molecular length (ca. 15 Å). The Bragg spacing (34.3 Å) corresponding to the peak at $Q \approx 0.183$ Å^{-1} is comparable to the bimolecular length. The large cross-sectional sizes of the OBHA fibers (using SANS and SAXS data) indicate that the mechanism of aggregation involves complex molecular associations. The hydroxylated parts of the molecules, which usually behave as chelating claws in this class of compounds,[13] are involved in hydrogen bonds, while the aliphatic chains, standing in reverse configuration, modulate the fiber−fiber interactions in the network.

The primary aggregates in OBHA organogels result from the stacking of head to head bimolecules associated by H-bonds. The network is made of bimolecular ribbons or fibrils fused in junction zones to form thicker fibers having one of the cross-sectional dimensions that is a multiple of the bimolecular length (the representation does not prejudge the related crystallographic space group). The microdomains generate both the Debye−Bueche scattering contribution in the low-angle region and the large-angle Bragg peak.

When the concentration is increased, the network increases its connectivity and consequently the number of its heterogeneities and related sizes. Experimentally, the scattering profile varies towards a Q^{-2}-decay, typical of flat ribbons or lamellar-like particles, as shown with SAXS (Figure 2 and analysis) and SANS (Figure 3 and analysis).

The description questions the existence of thinner fibers in the network. The analysis of the hypothesis requires the evaluation of the theoretical scattering of a two-population system made of cylindrical fibers ($r = 50$ Å for comparisons with SAXS data) and thinner fibrils ($r = 17.5$ Å). Figure 10 shows that such a system exhibits several characteristic features: (i) additional sharp decay (at ca. 0.2 Å^{-1}) due to the thin fibrils , (ii) damping of the first cross-sectional intensity decay of the thicker component (around ca. $Q \approx 0.1$ Å^{-1}), and (iii) enhancement of the intensity in between the two cross-sectional form factor oscillations. An illustration of the agreement obtained with such a two-population model is given in Figure 8 (curve 2). The existence of bimolecular fibrils is compatible with the present scattering data, while the hypothesis cannot be demonstrated to be unique. As mentioned in the Introduction, there is no driving force in organic liquids comparable to the hydrophobic effect in aqueous solutions that forces amphiphiles to aggregate in monodisperse structures. A coexistence of fibers with different populations of cross sections is probable (related to different multiples of the bimolecular length).

The network crystallinity is related to the proportion of fibers to nodes in the system. Such information could be attainable in future work by a concentration study of both the wide-angle Bragg peak(s) profiles and the variation of the low-angle prefactor for fiber scattering. The present study suggests that the molecular ordering in OBHA organogels is close to that of the crystalline solid phase, but not identical, so that unidirectional growth[3] can develop. Eventually, the shrinking phenomenon of the most dilute gels depends also upon the gel crystallinity. A loose network is more sensitive to fiber−fiber attractions than concentrated gels. The description proposed for OBHA organogels is certainly applicable to some other crystalline gels.

Acknowledgment. Drs. C. Williams, J. P. Lesieur (LURE), and J. Teixera (LLB) are thanked for their support during the scattering experiments. Dr. M. Bardet is acknowledged for his help during the NMR experiments.

Appendix

The low-angle scattering of OBHA dilute gels is described by the sum of the form factor (or combination of form factors if several geometries coexist) of unidirectional aggregates

(cylindrical fibers or ribbons) and a Debye−Bueche component related to the random distribution of the heterogeneities. The intensity reads as the sum of expressions 1 and 3. The OBHA network is assumed to be made up of fibers with a more or less circular cross section ($r = 50$ Å for comparisons with SAXS data), and a Gaussian distribution function ($\epsilon = \Delta r/r = 0.1$) takes into account both the polydispersity of the diameters and the instrumental resolution. The influence of the gelator concentration upon the low-angle part of the scattering is illustrated in Figure 11, which simulates the growth of both nodes (correlation length d and volume fraction ϕ_{nodes}) and fibers ($\phi_{\text{fibers}} = 1-\phi_{\text{nodes}}$).

The heterogeneities of the network are made of aggregated fibers that behave mechanically as nodes. In Figure 11A, ϕ_{nodes} is kept constant to 0.05 while d is varied. In Figure 11B, d is fixed to 500 Å while ϕ_{nodes} is varied. It is clearly seen that the effects of a change of either the fraction of nodes or their characteristic size d can be very important for the innermost part of the scattering curve.

References and Notes

(1) Mukkamala, R.; Weiss, R. G. *Langmuir* **1996**, *12*, 1474.
(2) Terech, P. In *Specialist surfactants*; Robb, I., Ed.; Chapman & Hall: London, 1997: Chapter 8, pp 208−268.
(3) Tachibana, T.; Mori, T.; Hori, K. *Bull. Chem. Soc. Jpn*. **1980**, *53*, 1714; **1981**, *54*, 73.
(4) Terech, P.; Rodriguez, V.; Barnes, J. D.; McKenna, G. B. *Langmuir* **1994**, *10*, 3406.
(5) Campbell, J.; Kuzma, M.; Labes, M. *Mol. Cryst. Liq. Cryst.* **1983**, *95*, 45.
(6) Hanabusa, K.; Okui, K.; Karaki, K.; Koyama, T.; Shirai, H. *J. Chem. Soc., Chem. Commun.* **1992**, 1371.
(7) Yamasaki, S.; Tsutsumi, H. *Bull. Chem. Soc. Jpn*. **1994**, *67*, 906.
(8) Terech, P.; Ramasseul, R.; Volino, F. *J. Phys. (Paris)* **1985**, *46*, 895.
(9) Wade, R. H.; Terech, P.; Hewat, E. A.; Ramasseul, R.; Volino, F. *J. Colloid Interface Sci.* **1986**, *114* (2), 442.
(10) Lin, Y.-c.; Kachar, B.; Weiss, R. G. *J. Am. Chem. Soc* **1989**, *111*, 5542.
(11) Mukkamala, R.; Weiss, R. G. *J. Chem. Soc., Chem. Commun.* **1995**, 375.
(12) Murata, K.; Aoki, M.; Susuki, T.; Harada, T.; Kawabata, H.; Komori, T.; Ohseto, F.; Ueda, K.; Shinkai, S. *J. Am. Chem. Soc*. **1994**, *116*, 6664.
(13) Chatterjee, B. *Coord. Chem. Rev.* **1978**, *26*, 281.
(14) Terech, P.; Wade, R. H. *J. Colloid Interface Sci.* **1988**, *125* (2), 542.
(15) Kratky O. *Prog. Colloid Polym. Sci.* **1988**, *77*, 1.
(16) Windsor, C. G. *J. Appl. Crystallogr.* **1988**, *21*, 582.
(17) Smith, W. L.; Raymond, K. N. *J. Am. Chem. Soc.* **1980**, *102* (4), 1252.
(18) Lindner, P.; Zemb, T. *Neutron, X-rays and light scattering: Introduction to an investigate tool for colloidal and polymeric systems;* North Holland-Elsevier: Amsterdam, 1991.
(19) Pimentel, G. C., McClellan, A. C. In *The hydrogen bond*; W. H. Freeman: San Francisco, CA, 1960.
(20) Almdal, K.; Dyre, J.; Hvidt, S.; Kramer, O. *Polym. Gels Networks* **1993**, *1*, 5.
(21) Guinier, A.; Fournet, G. *Small Angle Scattering of X-rays*; Wiley: New York, 1955.
(22) Cabane, B. In *Surfactant solutions;* Zana, R., Ed.; Surfactant Science Series 22; Marcel Dekker Inc.: New York, 1987; p 57.
(23) Glatter, O.; Kratky, O. In *Small angle X-ray scattering*; Academic Press: London, 1982.
(24) Debye, P.; Bueche, A. M. *J. Appl. Phys.* **1949**, *20*, 518.
(25) Mukherjee, K.; Moulik, S. P. *Langmuir* **1993**, *9*, 1727.
(26) Ruckenstein, E.; Nagarajan, R. *J. Phys. Chem.* **1980**, *84*, 1349.
(27) Israelachvili, J. N. *Intermolecular and surface forces*, 3rd ed.; Academic Press: London, 1992; p 341.
(28) Ferry, J. D. In *Viscoelastic Properties of Polymers*, 3rd ed.; Wiley: New York, 1980.